Supplementary Table 1. Clinical and neuropathological characteristics of controls and Alzheimer's disease (AD) patients included in the postmortem histological study. Abbreviations: CAA, cerebral amyloid angiopathy; CERAD, Consortium to Establish a Registry for Alzheimer's disease; F, female; M, male; MMSE, Mini-Mental State Examination; PMI, postmortem interval.

Patient Number	Diagnosis	Age	Gender	PMI (hr)	Vascular Risk Factors	Braak	CERAD	MMSE	Source
907	Control	84	M	3	None	I–II	Negative	28	USC ADRC
804	Control	82	M	9	None	0	Negative	28	USC ADRC
877	Control	93	M	3.75	None	I	Sparse	18	USC ADRC
720	Control	63	M	3.5	Hypertension	0	Negative	Unknown	USC ADRC
10473384	Control	84	M	5	Hypertension	III	Negative	26	Rush ADRC
20683921	Control	85	F	6	Hypertension	III	Sparse	26	Rush ADRC
20993308	Control	83	F	1	None	I	Negative	26	Rush ADRC
11072071	Control	88	M	8.5	Hypertension	II	Negative	27	Rush ADRC
15844425	Control	77	M	8	Hypertension	III	Negative	28	Rush ADRC
11342432	Control	90	M	2.5	None	II	Negative	29	Rush ADRC
11190734	Control	77	M	4.5	None	II	Negative	27	Rush ADRC
10383017	Control	88	F	5	Hypertension	I	Negative	27	Rush ADRC
20998065	Control	82	M	8.5	None	I	Negative	28	Rush ADRC
11697592	Control	78	M	9.75	None	I	Sparse	29	Rush ADRC
20800682	Control	85	F	5.75	None	II	Negative	30	Rush ADRC
800	AD	96	F	5	Atherosclerosis, CAA	V	Frequent	Unknown	USC ADRC
689	AD	78	F	7	None	V	Moderate	Unknown	USC ADRC
851	AD	87	F	4.75	Atherosclerosis	V	Frequent	16	USC ADRC
808	AD	98	M	6	Hypertension, CAA	V–VI	Frequent	28	USC ADRC
910	AD	100	F	4.75	Atherosclerosis	IV	Moderate	11	USC ADRC
911	AD	88	M	7	Atherosclerosis	III	Moderate	19	USC ADRC
915	AD	86	F	7.5	Atherosclerosis, CAA	V	Frequent	Unknown	USC ADRC
20195344	AD	94	F	5	Hypertension	IV	Moderate	11	RUSH ADRC
10248033	AD	88	M	18	Hypertension	III	Moderate	12	RUSH ADRC
11606935	AD	98	M	4	Hypertension	III	Moderate	18	RUSH ADRC
21403995	AD	86	F	21	Hypertension	III	Frequent	15	RUSH ADRC
20865035	AD	101	F	8.75	Hypertension	IV	Moderate	19	RUSH ADRC
20254902	AD	94	M	6	Hypertension	IV	Moderate	24	RUSH ADRC
20187042	AD	84	F	13	Hypertension	III	Moderate	22	RUSH ADRC
20506587	AD	92	F	4.25	None	III	Moderate	Unknown	RUSH ADRC
11326252	AD	95	M	3.25	Hypertension	IV	Moderate	20	RUSH ADRC

Supplementary Table 2. List of markers used in human postmortem histological studies.

Primary Antibody/Lectin (manufacture, catalog#, dilution used)	**Secondary Antibody (manufacture, catalog#; dilution used)**
Pericyte Marker	
Goat anti-human platelet-derived growth factor receptor beta (PDGFRβ; R&D Systems, AF385; 1:100)	Alexa fluor 568-conjugated donkey anti-goat (Invitrogen, A-11057; 1:500)
Fibrinogen/Fibrin	
Rabbit anti-human fibrinogen (Dako, A0080; 1:500)	Alexa fluor 568-conjugated donkey anti-rabbit (Invitrogen, A-10042; 1:500)
Vasculature	
Dylight 488-conjugated *L. esculentum* lectin (Vector Labs, DL-1174; 1:200)	N/A
Myelin	
Mouse monoclonal anti-human myelin basic protein (MBP) (F-6) (Santa Cruz, sc-271524, 1:200)	Alexa fluor 647-conjugated donkey anti-mouse (Invitrogen, A-31571; 1:500)
Oligodendrocytes	
Rabbit polyclonal anti-mouse Olig2, react with human Olig2 (Millipore, AB9610, 1:200)	Alexa fluor 488-conjugated donkey anti-rabbit (Invitrogen, A-21206; 1:500)

Supplementary Table 3. List of markers used in mouse histological studies.

Primary Antibody/Lectin (manufacture, catalog#, dilution used)	Secondary Antibody (manufacture, catalog#; dilution used)
Pericyte Marker	
Goat anti-mouse aminopeptidase N/ANPEP (CD13; R&D systems, AF2335; 1:100)	Alexa fluor 488- or 568-conjugated donkey anti-goat (Invitrogen, A-11055 or A-11057; 1:500)
Goat anti-human platelet-derived growth factor receptor beta (PDGFRβ; R&D Systems, AF385; 1:100)	Alexa fluor 568-conjugated donkey anti-goat (Invitrogen, A-11057; 1:500)
Fibrinogen/Fibrin	
Rabbit anti-human fibrinogen (Dako, A0080; 1:500)	Alexa fluor 568-conjugated donkey anti-rabbit (Invitrogen, A-10042; 1:500)
Myelin	
Goat anti-human myelin basic protein (MBP; Santa Cruz, sc-13914-R; 1:500)	Alexa fluor 488- or 568-conjugated donkey anti-goat (Invitrogen, A-11055 or A-11057; 1:500)
Axons	
Mouse anti-mouse axonal SMI-312 neurofilament marker (SMI-312; BioLegend, SMI312; 1:500)	Alexa fluor 568-conjugated donkey anti-mouse (Invitrogen, A-10037; 1:500)
Oligodendrocytes	
Rabbit anti-mouse Olig2 (Millipore, AB9610; 1:200)	Alexa fluor 488- or 568-conjugated donkey anti-rabbit (Invitrogen, A-21206 or A-10042; 1:500)
Monoclonal mouse anti-Olig2 (ThermoFisher, MA5-15810; 1:200)	Alexa fluor 488- or 568-conjugated donkey anti-mouse (Invitrogen, A-21202 or A-10037; 1:500)
Mature Oligodendrocytes	
Mouse anti-cyclic nucleotide phosphodiesterase (CNPase; Abcam, ab6319; 1:500)	Alexa fluor 647-conjugated donkey anti-mouse (Invitrogen, A-31571; 1:500)
Oligodendrocyte Progenitor Cells	
Rabbit anti-platelet-derived growth factor receptor alpha (PDGFRα; Cell Signaling, #3174; 1:200)	Alexa fluor 568-conjugated donkey anti-rabbit (Invitrogen, A-10042; 1:500)
Neurons	
Rabbit anti-mouse NeuN (Millipore, ABN78; 1:500)	Alexa fluor 568- or 647-conjugated donkey anti-rabbit (Invitrogen, A-10042 or A-31573; 1:500)
Vasculature	
Dylight 488-conjugated *L. esculentum* lectin (Vector Labs, DL-1174; 1:200)	N/A
Microglia	
Rabbit anti-mouse ionized calcium binding adaptor molecule 1 (Iba-1; Wako, 019-19741; 1:1,000)	Alexa fluor 488-conjugated donkey anti-rabbit (Invitrogen, A-21206; 1:500)
Astrocytes	
Rabbit anti-Glial Fibrillary Acidic Protein (GFAP; Dako, z0334; 1:500)	Alexa fluor 647-conjugated donkey anti-rabbit (Invitrogen, A-31573; 1:500)
Flow Cytometry & In Vitro Mature Oligodendrocytes	

Rabbit anti-proteolipid protein (PLP; Abcam, ab105784; 1:2,000)	Alexa fluor 488-conjugated donkey anti-rabbit (Invitrogen, A-21206; 1:200)
Mouse anti-myelin basic protein (SMI-99; BioLegend; 1:500)	Alexa fluor 647-conjugated donkey anti-mouse (Invitrogen, A-21202 or A-31571; 1:200)

Supplementary Table 4. List of primers used for cytokine and chemokine expression levels.

Tnf-α	Forward	5'-CTTCTGTCTACTGAACTTCGGG-3'
	Reverse	5'-TGATCTGAGTGTGAGGGTCTG-3'
Il-6	Forward	5'-CAAAGCCAGAGTCCTTCAGAG-3'
	Reverse	5'-GTCCTTAGCCACTCCTTCTG-3'
Il-1β	Forward	5'-AAGGGCTGCTTCCAAACCTTTGAC-3'
	Reverse	5'-ATACTGCCTGCCTGAAGCTCTTGT-3'
Ccl2	Forward	5'-CATCCACGTGTTGGCTCA-3'
	Reverse	5'-GATCATCTTGCTGGTGAATCAGT-3'
Icam-1	Forward	5'-AAGGAGATCACATTCACGGTG-3'
	Reverse	5'-TTTGGGATGGTAGCTGGAAG-3'
18S rRNA	Forward	5'-GTAACCCGTTGAACCCCATT-3'
	Reverse	5'-CCATCCAATCGGTAGTAGCG-3'

Supp. Figure 1

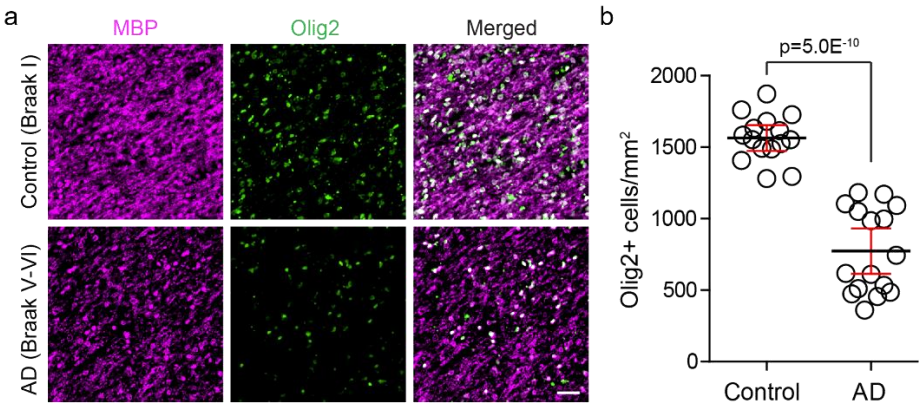

Supplementary Figure S1. Histopathological studies in the white matter of AD cases compared to controls. (**a**) Representative immunostaining for myelin basic protein (MBP) (magenta) and oligodendrocyte transcription factor Olig2 (green) in the prefrontal subcortical white matter of an age-matched control (Braak I, upper) and AD case (Braak V–VI, lower) (bar = 20 µm). (**b**) Quantification of Olig2-positive oligodendrocytes in the prefrontal subcortical white matter of controls (n=15) compared to AD (n=16). Mean ± s.e.m. See Supplementary Table 1 for demographic information. In panel b, unpaired two-tailed Student's *t*-test was used.

Supp. Figure 2

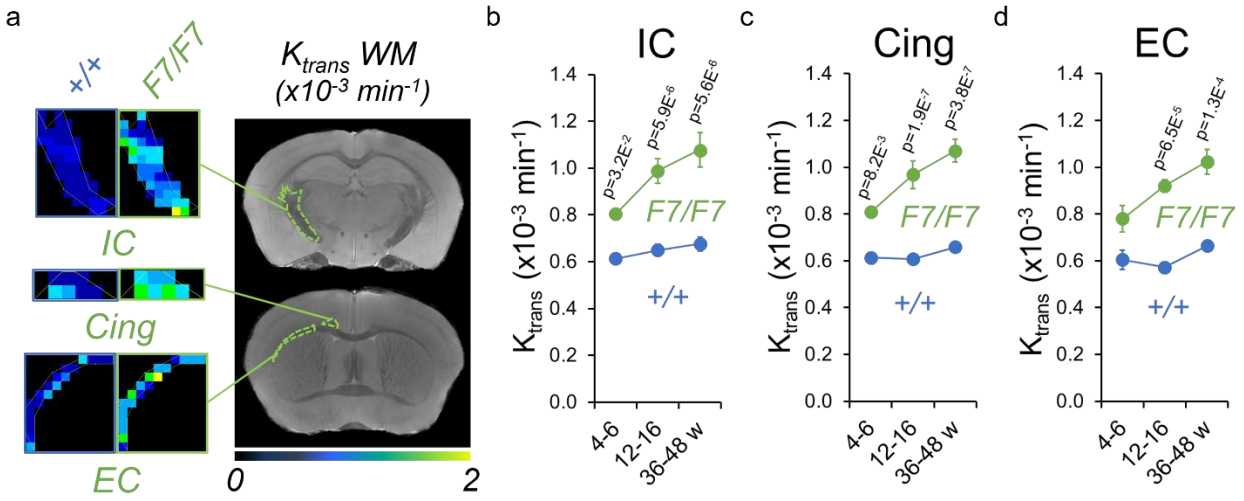

Supplementary Figure S2. Blood-axon barrier breakdown in the white matter tracts of pericyte-deficient mice. (**a**) The blood-axon barrier permeability constant (K_{trans}) maps in the white matter internal capsule (IC), cingulum (Cing), and external capsule (EC) regions generated from dynamic contrast-enhanced magnetic resonance imaging scans in 16-week old *F7/F7* and littermate control +/+ mice. (**b-d**) The regional K_{trans} values in IC (**b**), Cing (**c**) and EC (**d**) regions in 4-6-, 12-16-, and 36-48-week old *F7/F7* (green) and littermate control +/+ (blue) mice. Mean ± s.e.m.; n=6 4-6-week old mice per group; n=7 12-16-week old mice per group; n=5 36-48-week old mice per group. In panels b-d, one-way ANOVA and Bonferroni's post hoc tests were used.

Supp. Figure 3

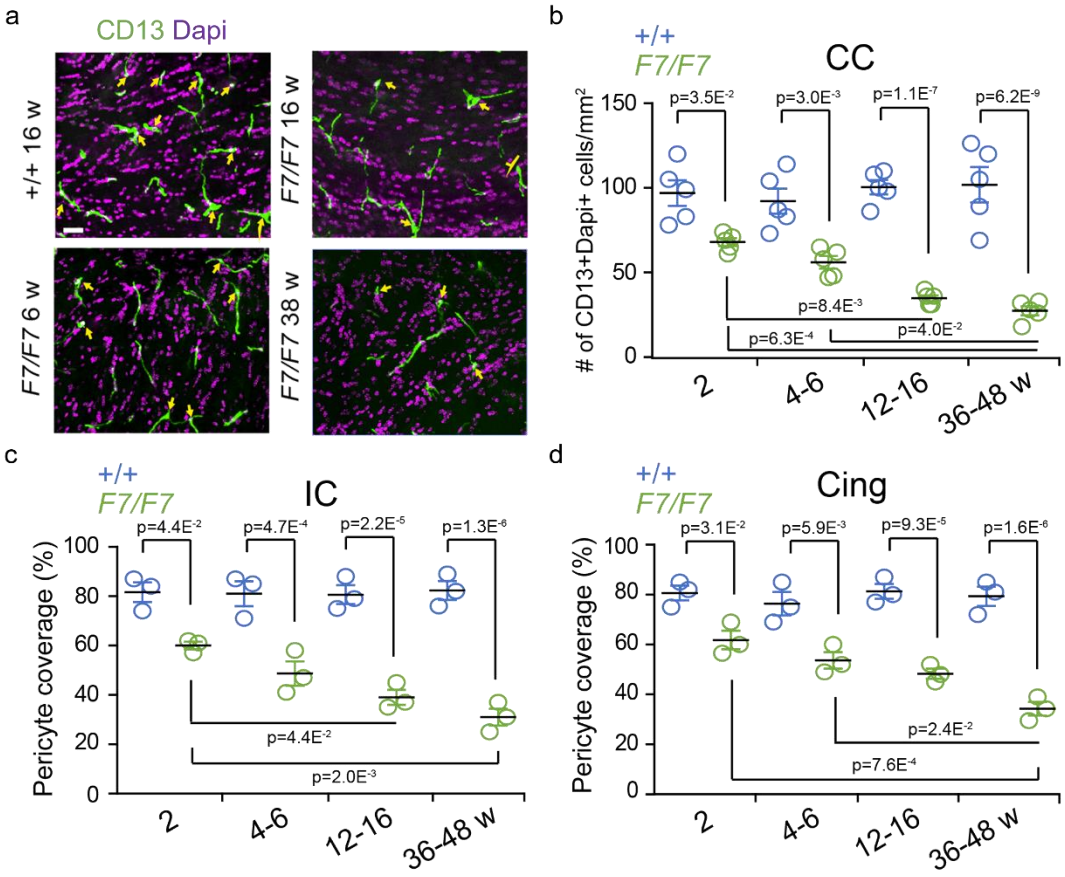

Supplementary Figure S3. Pericyte loss in the white matter of pericyte-deficient mice. (**a**) Representative confocal images of CD13-positive pericyte cell bodies co-localized with nuclear 4,6-Diamidino-2-phenylindole, dihydrochloride (Dapi) staining indicated by yellow arrows in the corpus callosum (CC) of 6-, 16- and 38-week old *F7/F7* and control 16-week old +/+ mice (bar = 40 µm). (**b**) Quantification of CD13-positive cell bodies colocalized with Dapi per mm^2 of tissue sections in CC in 2-, 4-6-, 12-16-, and 36-48-week old *F7/F7* (green) and littermate control (+/+, blue) mice. Mean ± s.e.m.; n=5 animals per group. (**c, d**) Progressive loss of pericyte coverage in the internal capsule (IC, **c**) and cingulum (Cing, **d**) of 2-, 4-6-, 12-16-, and 36-48-week old *F7/F7* (green) and +/+ control (blue) mice. Mean ± s.e.m.; n=3 mice per group. In panels b-d, one-way ANOVA and Bonferroni's post hoc tests were used.

Supp. Figure 4

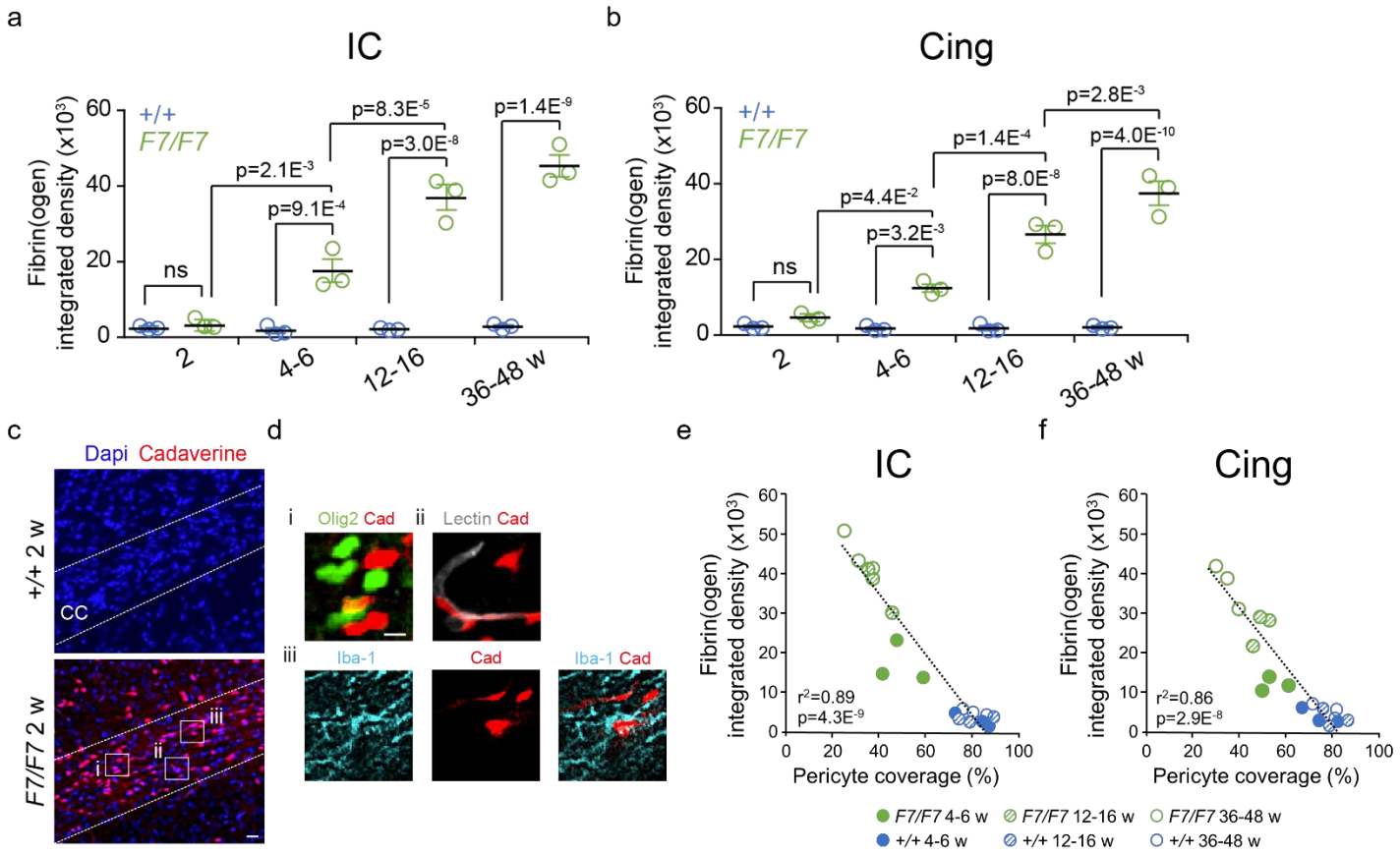

Supplementary Figure S4. Pericyte coverage and fibrin(ogen) deposits in the white matter tracts of pericyte-deficient mice. (**a, b**) Fibrin(ogen) leakage in the internal capsule (IC, **a**) and cingulum (Cing, **b**) of 2-, 4-6-, 12-16-, and 36-48-week old *F7/F7* (green) and control (+/+, blue) mice. Mean ± s.e.m.; n=3 mice per group. (**c**) Representative images of 5 independent replicates of the CC showing Dapi-positive nuclei (blue) and cellular uptake of Alexa Fluor 555-conjugated cadaverine (Cad, red) in 2-week old *F7/F7* and control (+/+) mice (bar = 20 µm). (**d**) Insets i-iii show cadaverine uptake by oligodendrocytes (i, Olig-2, green; Cad, cadaverine-positive cells), perivascular mural cells on endothelial lectin-positive vascular profiles (ii, Lectin, grey; Cad), and microglia (iii, Iba-1, green; Cad; bar = 10 µm). (**e, f**) Negative correlation between fibrin(ogen) extravascular deposits and pericyte coverage in the IC (**e**) and Cing (**f**); n=18 individual points from *F7/F7* and control (+/+) mice at different ages; r^2, Pearson's coefficient. In panels a and b, one-way ANOVA and Bonferroni's post hoc tests were used; ns=non-significant (p>0.05).

Supp. Figure 5

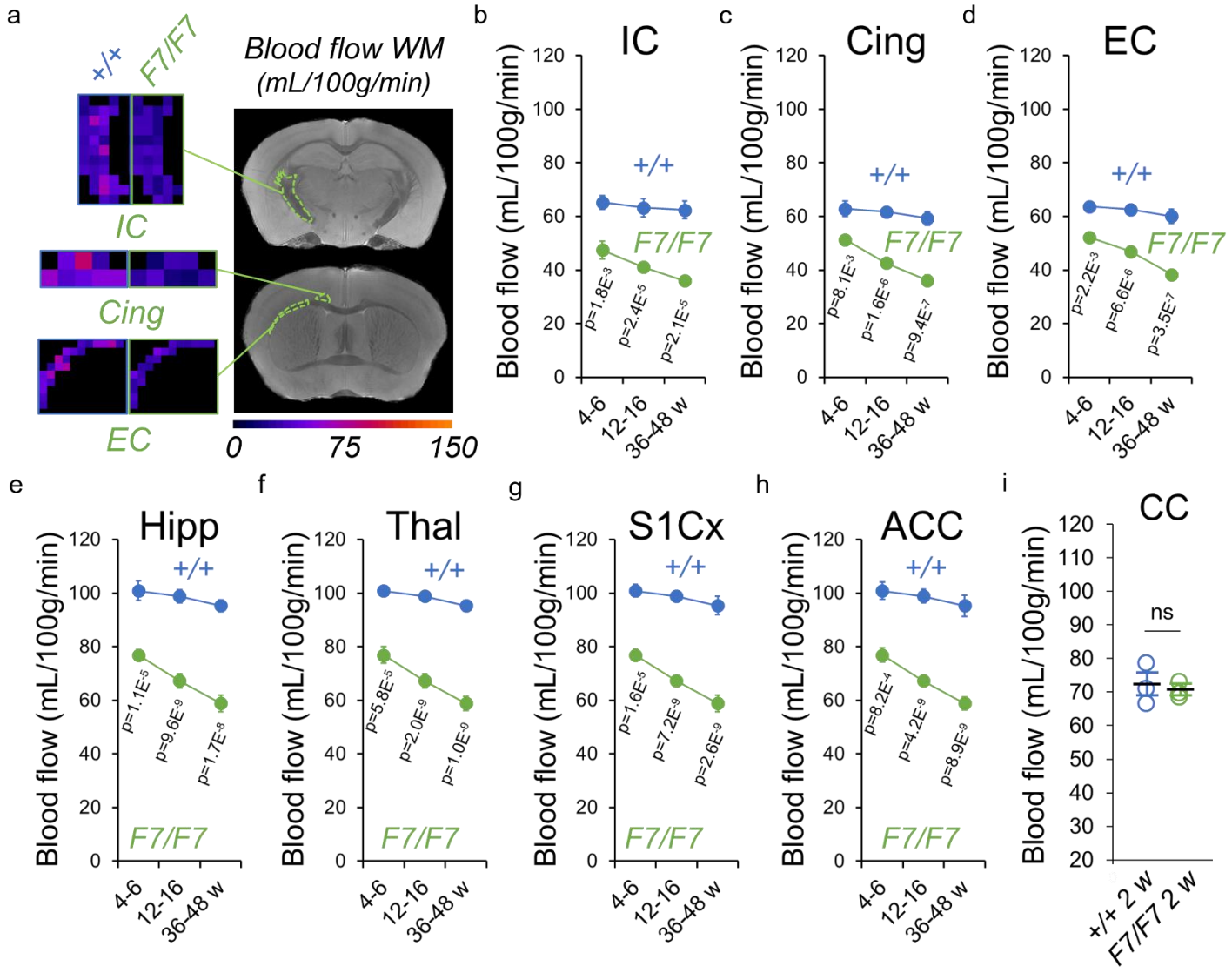

Supplementary Figure S5. Blood flow reductions in the white matter tracts compared to grey matter regions of pericyte-deficient mice. (**a**) The blood flow maps in the white matter internal capsule (IC), cingulum (Cing), and external capsule (EC) tracts generated from dynamic susceptibility-contrast magnetic resonance imaging scans in 16-week old *F7/F7* and littermate control +/+ mice. (**b-d**) The regional blood flow values in IC (**b**), Cing (**c**) and EC (**d**) in 4-6-, 12-16-, and 36-48-week old *F7/F7* (green) and littermate control +/+ (blue) mice. Mean ± s.e.m.; n=6 4-6-week old mice per group; n=7 12-16-week old mice per group; n=5 36-48-week old mice per group. (**e-h**) Blood flow in grey matter regions including dorsal hippocampus (Hipp, **e**), posterior thalamus (Thal, **f**), primary somatosensory barrel cortex (S1Cx, **g**), and anterior cingulate cortex (ACC, **h**) in 4-6-, 12-16-, and 36-48-week old *F7/F7* (green) and +/+ (blue) mice. Mean ± s.e.m.; n=6 4-6-week old mice per group; n=7 12-16-week old mice per group; n=5 36-48-week old mice per group. (**i**) The regional blood flow values in CC in 2-week old *F7/F7* (green) and littermate control (+/+, blue) mice. Mean ± s.e.m.; n=3 mice per group. In panels b-h, one-way ANOVA and Bonferroni's post hoc tests were used. In panel i, unpaired two-tailed Student's *t*-test was used; ns=non-significant (p>0.05).

Supp. Figure 6

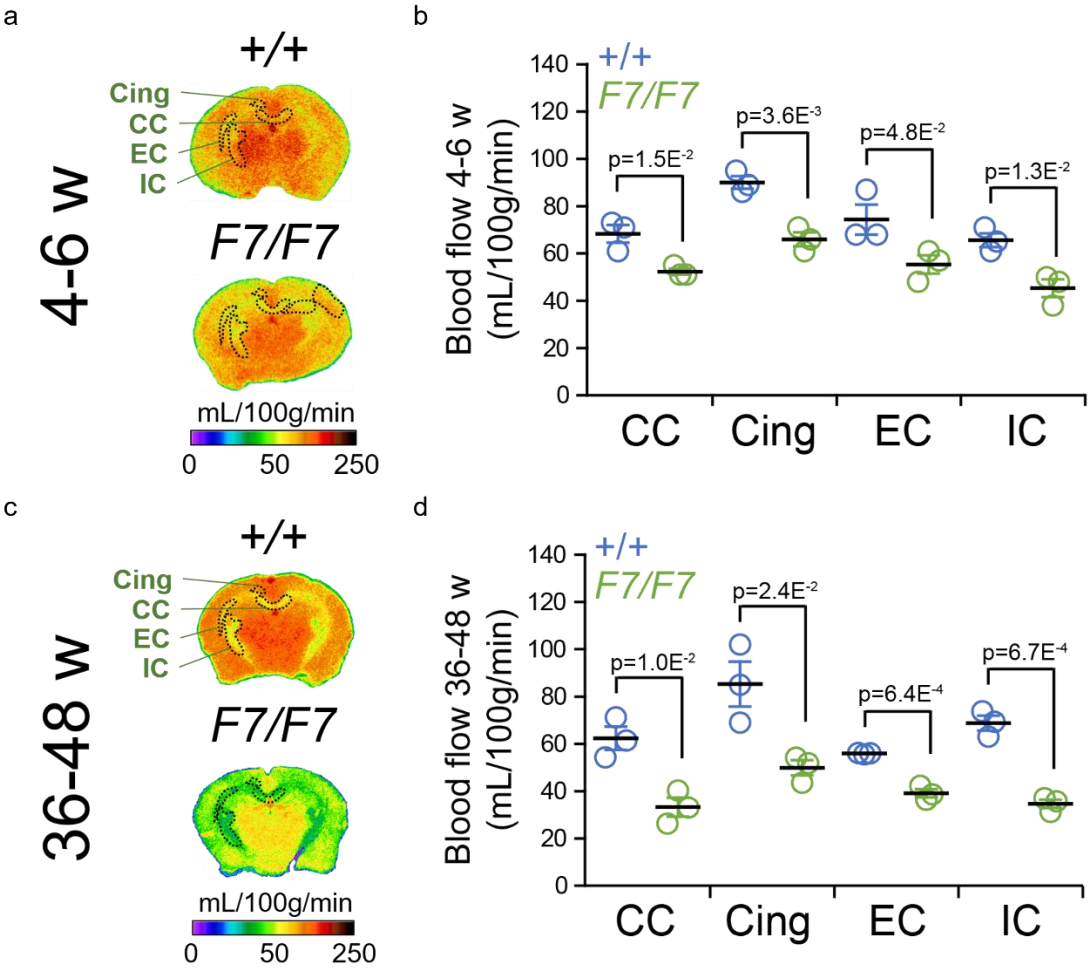

Supplementary Figure S6. ^{14}C-iodoantipyrine (IAP) autoradiography measurements of blood flow in the white matter of pericyte-deficient mice. Representative ^{14}C-IAP autoradiography blood flow maps in 4-week old (**a**) and 48-week old (**c**) *F7/F7* (*lower*) and age-matched +/+ control (+/+, *upper*) mice. Quantitative ^{14}C-IAP autoradiography in white matter regions including corpus callosum (CC), cingulum (Cing), external capsule (EC), and internal capsule (IC) in 4-6-week old (**b**) and 36-48-week old (**d**) *F7*/F7 (green) and +/+ (blue) mice. Mean ± s.e.m.; n=3 mice per group. In panels b and d, unpaired two-tailed Student's *t*-tests were used.

Supp. Figure 7

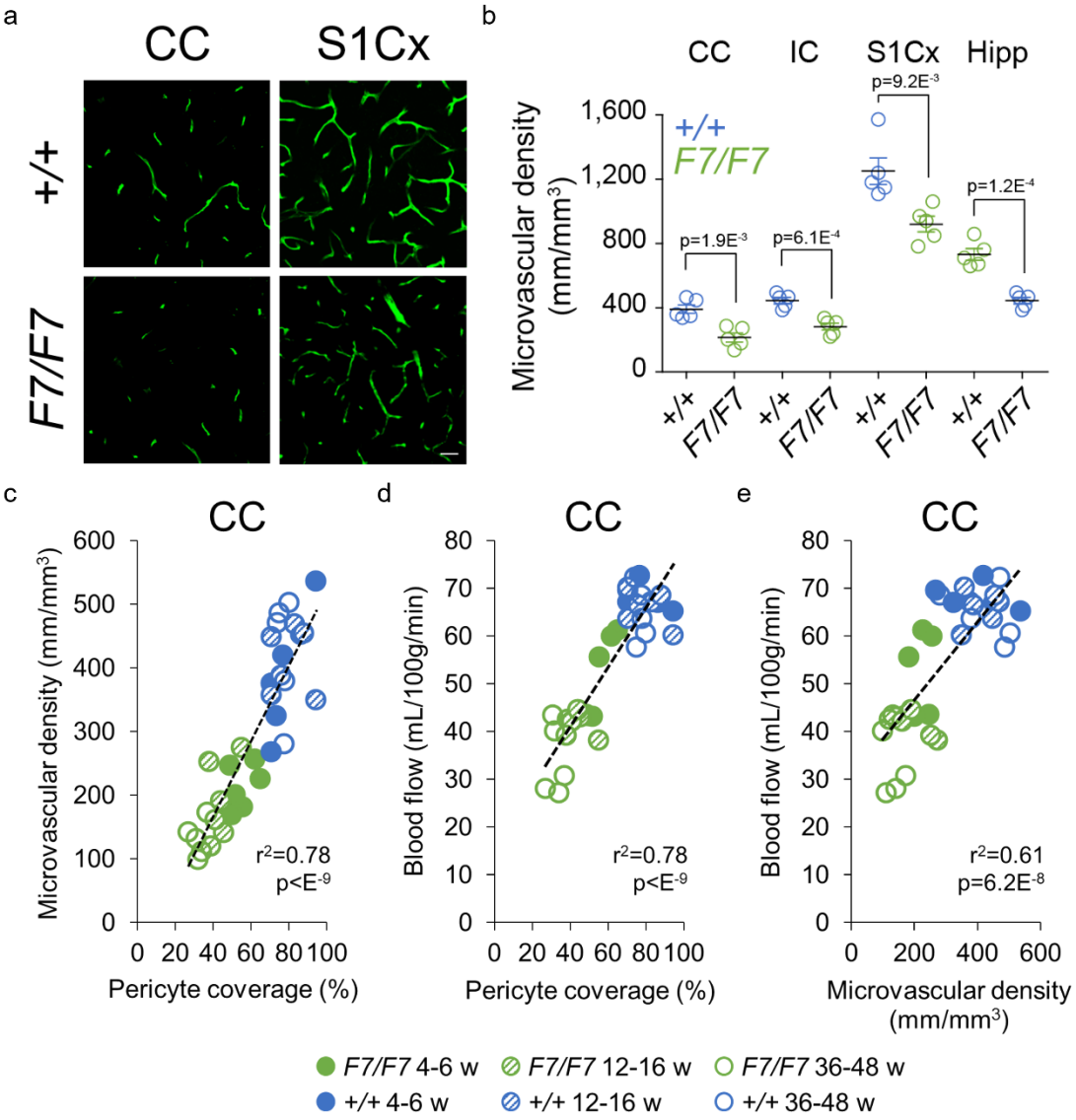

Supplementary Figure S7. Microvascular reductions in the white matter relative to grey matter regions in pericyte-deficient mice. (**a**) Lectin-positive endothelial profiles showing the microvascular density in the white matter corpus callosum (CC) compared to grey matter primary somatosensory cortex (S1Cx) in 16-week old *F7/F7* and +/+ mice (bar = 20 µm). (**b**) Quantification of microvascular density in white matter CC and internal capsule (IC) tracts compared to grey matter S1Cx and dorsal hippocampus (Hipp) regions in 12-16-week old *F7/F7* and +/+ mice. Mean ± s.e.m.; n=5 mice per group. (**c-e**) Positive correlations between microvascular density and pericyte coverage (**c**), blood flow and pericyte coverage (**d**), and blood flow and microvascular density (**e**) in the CC; n=36 individual points from *F7/F7* and +/+ mice at different ages; r^2, Pearson's coefficient. In panel b, unpaired two-tailed Student's *t*-tests were used.

Supp. Figure 8

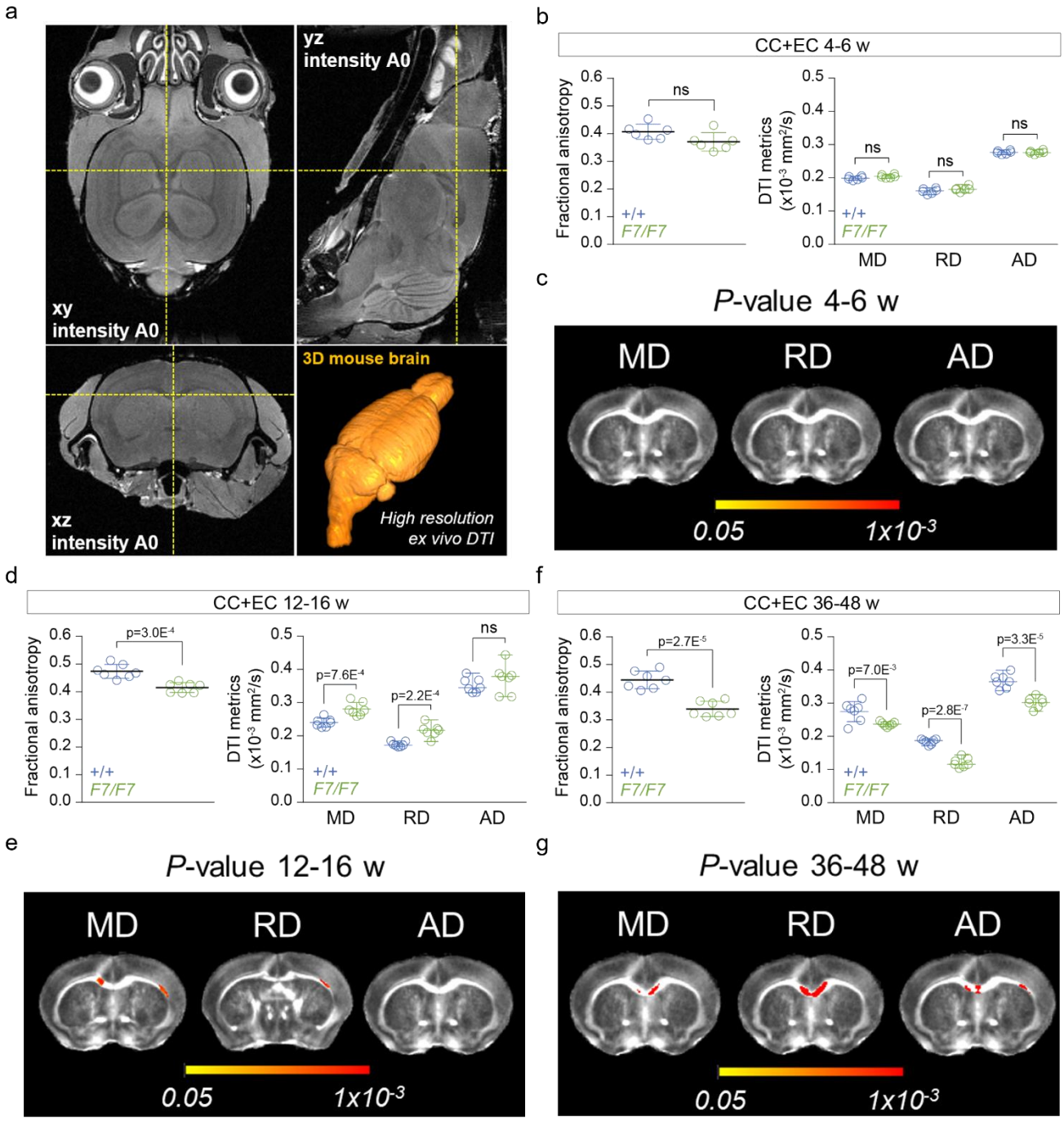

Supplementary Figure S8. Changes in the white matter tracts detected by high-resolution diffusion tensor imaging (DTI) in pericyte-deficient mice. (**a**) Intensity A0 images with 80 µm isotropic resolution showing horizontal (*top left*), sagittal (*top right*), and coronal (*bottom left*) sections, and a 3D reconstruction of a 16-week old *F7/F7* brain (*bottom right*). In **b**, **d**, and **f**, DTI metrics including fractional anisotropy (FA), mean diffusivity (MD), radial diffusivity (RD), and axial diffusivity (AD) were measured in pooled corpus callosum (CC) and external capsule (EC) samples in 4-6-week (**b**), 12-16-week (**d**), and 36-48-week (**f**) old *F7/F7* (green) mice compared to +/+ (blue) controls. In **c**, **e**, and **g**, probabilistic *P*-value maps for MD, RD, and AD computed from DTI scans in 4-6-week (**c**), 12-16-week (**e**), and 36-48-week (**g**) old *F7/F7* mice were compared to +/+ controls. Yellow-Red voxels, statistically significant changes in white matter regions in *F7/F7* mice compared to their age-matched +/+ littermate controls by searchlight-based multivoxel pattern analysis (see Online Methods). Mean ± s.d.; n=6 4-6-week old mice per group; n=7 12-16-week old mice per group; n=7 36-48-week old mice per group. In panels, b, d, and f, unpaired two-tailed Student's *t*-tests were used; ns=non-significant (p>0.05).

Supp. Figure 9

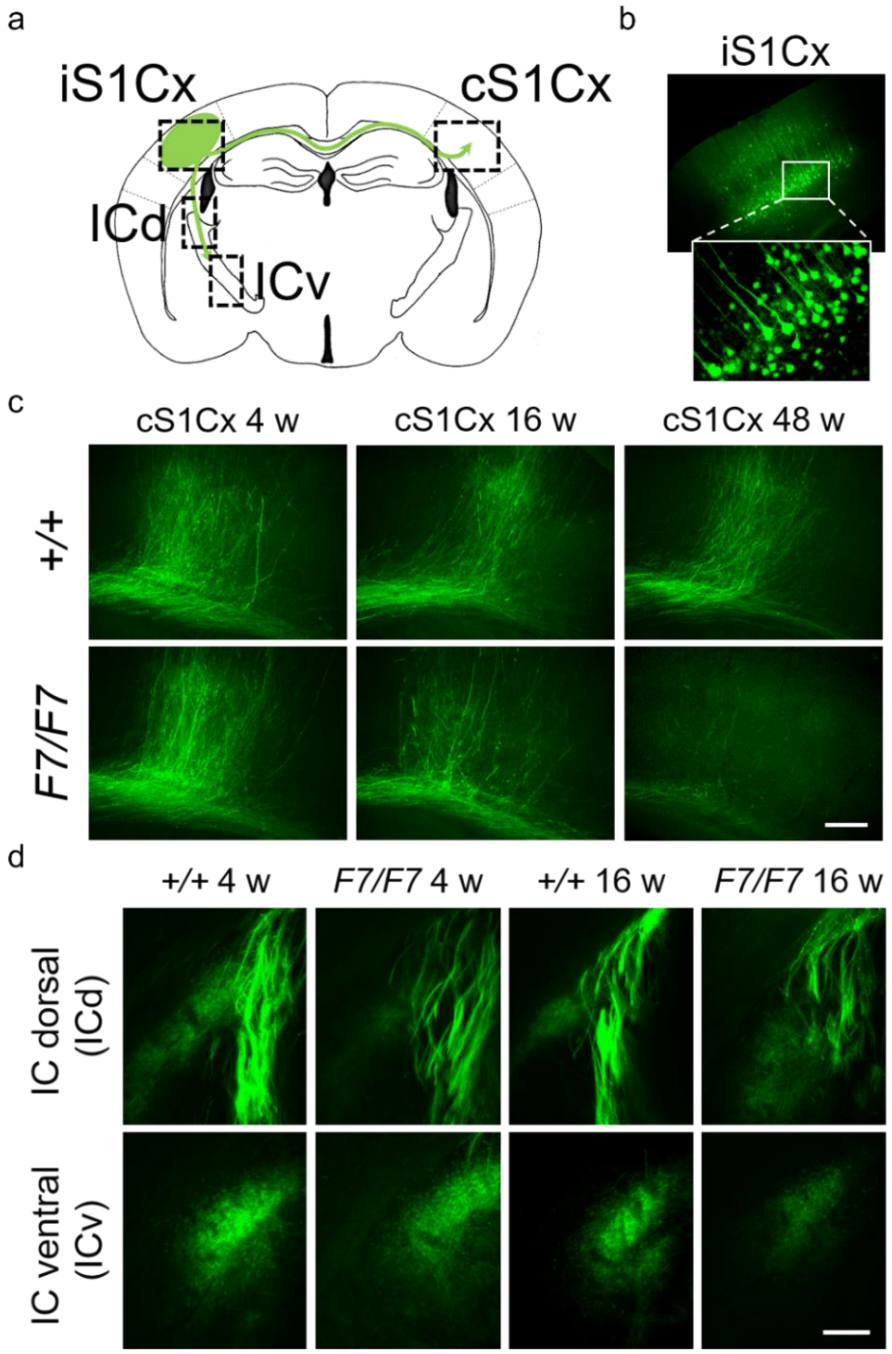

Supplementary Figure S9. Viral-based tract-tracing connectomics in pericyte-deficient mice. Anterograde tract-tracing using an adeno-associated virus expressing green fluorescent protein (AAV-eGFP) was performed in 4-6-, 12-16-, and 36-48-week old *F7/F7* and control (+/+) mice (n=5 mice per group). (**a**) A diagram showing the injection site, the ipsilateral primary somatosensory barrel cortex (iS1Cx), and fiber projections towards the dorsal and ventral IC (ICd and ICv, respectively) and the contralateral S1Cx (cS1Cx) through the corpus callosum. (**b**) The injection site shows cortical neurons labeled with the AAV-eGFP (one section plane). (**c**) 3D-projections in *F7/F7* mice show progressively reduced projection density of the labeled-virus within the cS1Cx compared to +/+ controls 21 days after labeling in 4-, 16-, and 48-week old animals (bar = 100 µm). (**d**) 3D-projections in *F7/F7* mice also show progressively reduced projection density of the labeled-virus within the ICd (*upper*) and ICv (*lower*) compared to +/+ controls in 4- and 16-week old mice (bar = 100 µm).

Supp. Figure 10

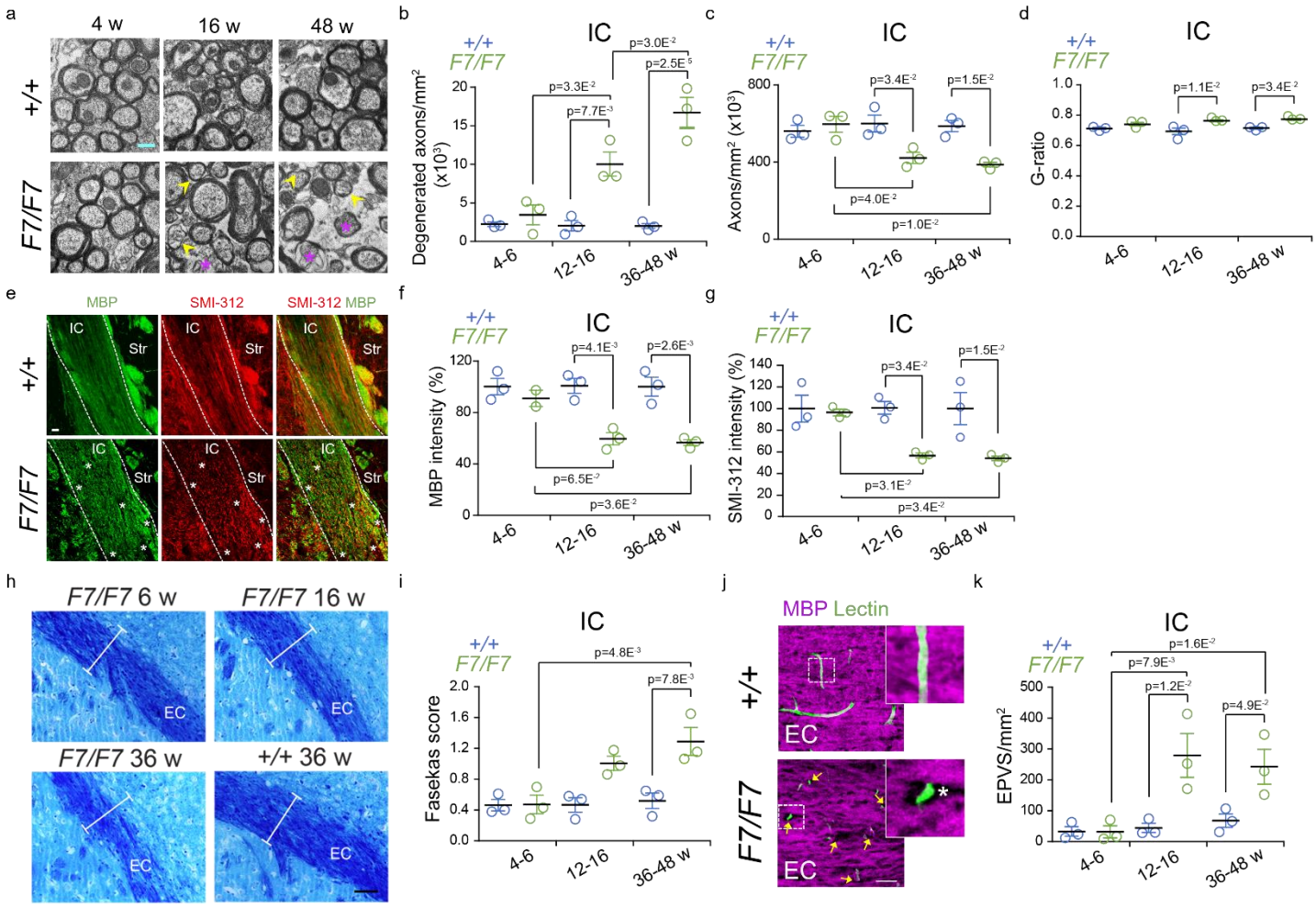

Supplementary Figure S10. Histological tissue analysis of microstructural changes in the white matter tracts of pericyte-deficient mice. (**a**) Electron microscopy images of the internal capsule (IC) in 4-, 16-, and 48-week old *F7/F7* and +/+ mice. Yellow arrowheads, thinner myelin sheaths; purple stars, degenerated axons (bar = 0.5 µm). (**b-d**) Quantification of the number of degenerated axons (**b**), total number of axons (**c**), and g-ratio (**d**) in 4-6-, 12-16-, and 36-48-week old *F7/F7* (green) and control (+/+, blue) mice. Mean ± s.e.m.; n=3 mice per group. (**e**) Immunostaining of MBP and SMI-312 in the IC of 16-week old *F7/F7* and control (+/+) mice (bar = 20 µm); dotted lines, IC delineation; Str, striatum; stars show MBP and SMI-312 loss. (**f, g**) Quantification of MBP (**f**) and SMI-312 (**g**) immunoreactivity in 4-6-, 12-16-, and 36-48-week old *F7/F7* (green) and +/+ (blue) mice. Mean ± s.e.m.; n=3 (+/+) and 2 (*F7/F7*) 4-6-week old mice per group; n=3 12-16-week old mice per group; n=3 36-48-week old mice per group. (**h**) Luxol fast blue and cresyl violet staining in the external capsule (EC) of 6, 16 and 36-week old *F7/F7* mice compared to 36-week old +/+ control (bar = 100 µm). White bar in each panel shows the thickness of the external capsule determined in 36-week old +/+ control mouse (*lower right panel*) and shown in each panel for comparison. (**i**) Fazekas score of white matter damage in the EC of 4-6-, 12-16-, and 36-48-week old *F7/F7* (green) and +/+ (blue) control mice. Mean ± s.e.m.; n=3 mice per group. (**j**) Immunostaining for MBP and endothelial lectin in the EC of 16-week old *F7/F7* and +/+ mice (bar = 20 µm); yellow arrows, enlarged perivascular spaces (EPVS). Insets denote high magnification boxed regions; white star, EPVS. (**k**) Quantification of the number of EPVS per mm^2 tissue in the EC of 4-6-, 12-16-, and 36-48-week old *F7/F7* (green) and +/+ (blue) mice. Mean ± s.e.m.; n=3 mice per group. In panels b-d, f, g, i, and k, one-way ANOVA and Bonferroni's post hoc tests were used.

Supp. Figure 11

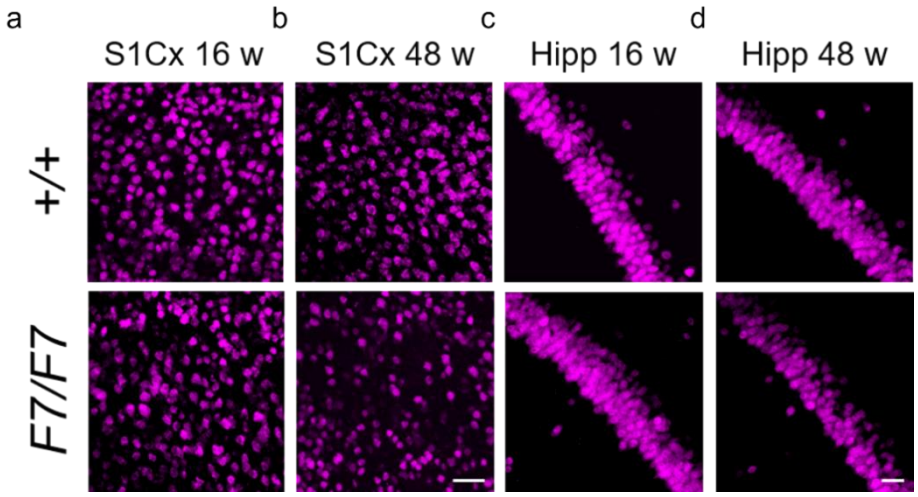

Supplementary Figure S11. NeuN-positive neurons in the cortex and hippocampus of pericyte-deficient mice. Confocal images of NeuN (neuronal marker)-positive cells in the primary somatosensory cortex (S1Cx; layer IV-V) and hippocampus CA1 subfield in 16-week old (**a, c**) and 48-week old (**b, d**) *F7/F7* and +/+ control mice (bar = 20 µm); Images are representative of 3 mice per group.

Supp. Figure 12

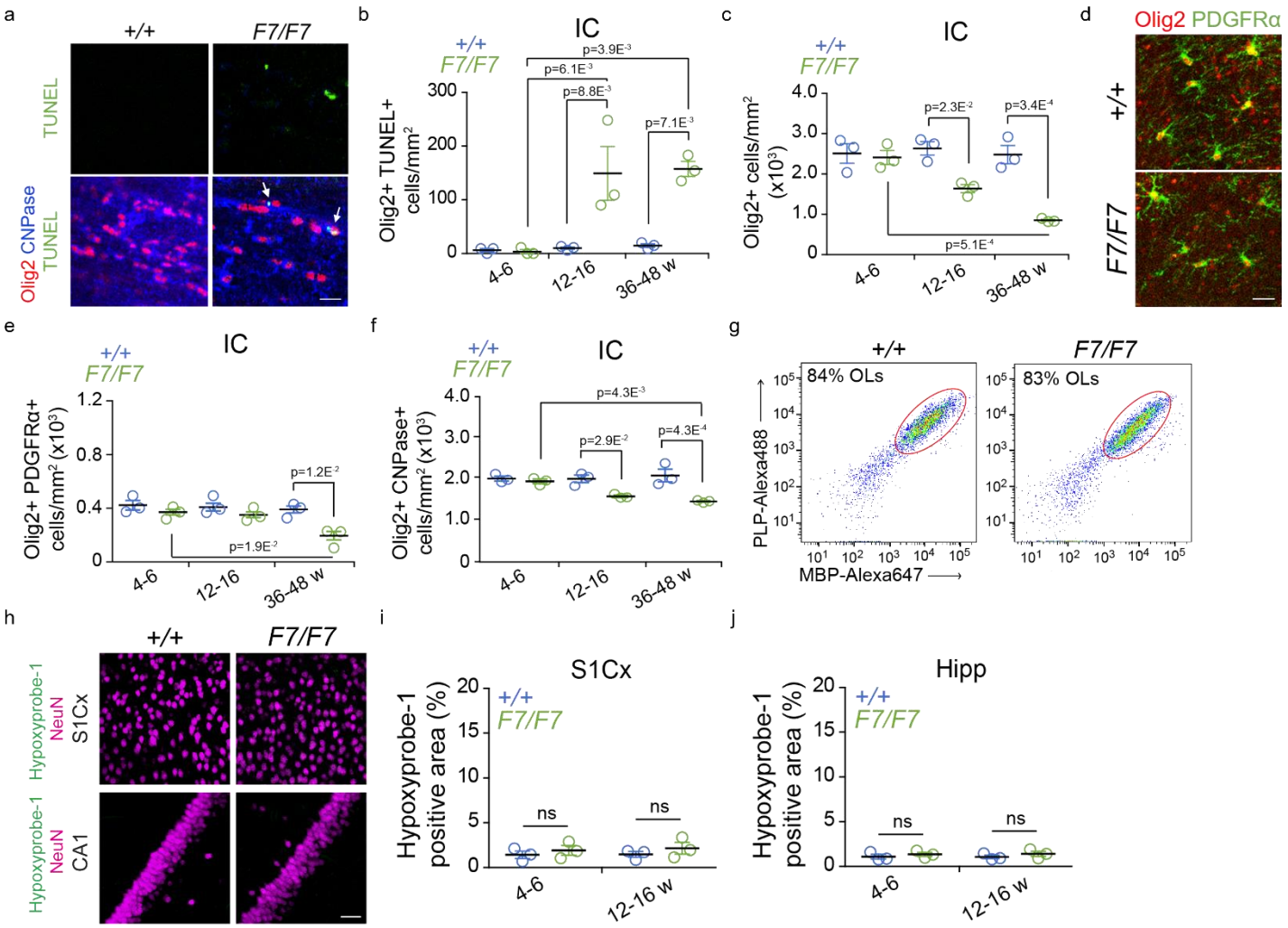

Supplementary Figure S12. Loss of mature oligodendrocytes in the white matter tracts of pericyte-deficient mice. (**a-c**) Confocal images (**a**, bar = 20 µm) of Olig2 (oligodendrocyte marker), CNPase (mature oligodendrocyte marker), and TUNEL staining in the internal capsule (IC) of 16-week old *F7/F7* and +/+ mice. Arrows, Olig2- and TUNEL-double positive cells. Number of Olig2- and TUNEL- double positive cells (**b**) and Olig2-positive cells (**c**) in the IC of *F7/F7* (green) and +/+ control (blue) mice. Mean ± s.e.m.; n=3 mice per group. (**d-f**) Confocal images (**d**, bar = 20 µm) of Olig2- and PDGFRα- (oligodendrocyte progenitor cell marker) double positive cells in the IC of 16-week old *F7/F7* and +/+ mice, and quantification of Olig2- and PDGFRα-double positive oligodendrocyte progenitor cells (**e**) and Olig2- and CNPase-double positive myelinated mature oligodendrocytes (**f**) in the IC of 4-6-, 12-16-, and 36-48-week old *F7/F7* (green) and +/+ (blue) control mice. Mean ± s.e.m.; n=3 mice per group. (**g**) Flow cytometry analysis of MBP-Alexa647- and PLP-Alexa488-double positive myelinated mature oligodendrocytes isolated from white matter. Representative dot plots are from 3 independent experiments in 4-6-week old *F7/F7* and +/+ control mice. (**h-j**) Confocal analysis of hypoxyprobe-1 (pimonidazole)-positive hypoxic tissue (O_2<10 mmHg) in the primary somatosensory barrel cortex (S1Cx) and hippocampus CA1 subfield of 16-week old *F7/F7* and +/+ control mice (**h**, bar = 20 µm), and quantification of hypoxyprobe-1-positive area expressed as the percentage of total tissue in the S1Cx (**i**) and hippocampus (Hipp; **j**) in 4-6 and 12-16-week old *F7/F7* (green) and +/+ (blue) control mice. Mean ± s.e.m.; n=3 mice per group. In panels b, c, e, f, i, and j, one-way ANOVA and Bonferroni's post hoc tests were used; ns=non-significant (p>0.05).

Supp. Figure 13

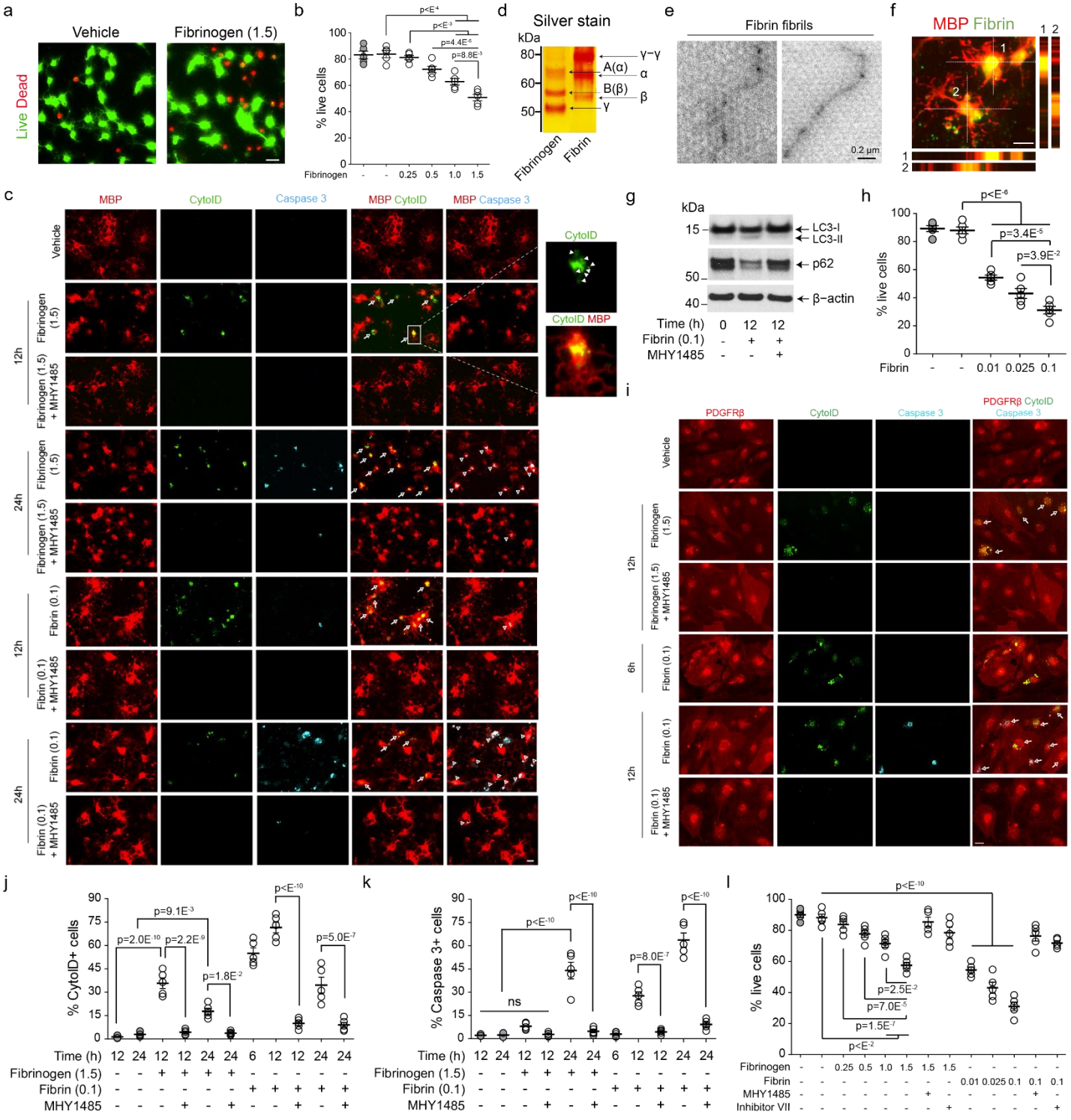

Supplementary Figure S13. Autophagy-dependent cell death in mouse oligodendrocyte and pericyte cultures after treatment with fibrinogen and fibrin fibrils. (**a**) Representative confocal images showing live (green) and dead (red) mature oligodendrocytes (OLs) by live/dead assay 24h after vehicle or fibrinogen treatment (1.5 mg/mL). Bar = 10 μm. (**b**) Quantification of live OLs assessed by live/dead assay 24h after vehicle and fibrinogen (0.25-1.5 mg/mL) treatment. In all studies, hirudin (4 U/mL) was added to the cultures to block a possible cell-associated thrombin activity (open circles). Grey filled circles – control-vehicle with no hirudin. Mean ± s.e.m.; n=5 independent experiments (each 3 coverslips per condition). (**c**) Representative confocal images of OLs after treating live cells with CytoID autophagy kit (green, middle) followed by immunostaining for myelin basic protein (MBP) (red, left) and cleaved, active form of caspase 3 (cyan, right) at 12 and 24 h of vehicle,

fibrinogen (1.5 mg/mL) or fibrin (0.1 mg/mL) treatment with and without MHY 1485 (2 μM), a mTOR activator which inhibits autophagy. Arrows point to formation of autophagosomes in MBP and CytoID double-positive OLs; arrowheads point towards MBP and Caspase 3 double-positive OLs (bar = 10 μm). Inset, a magnified MBP and CytoID double-positive cell with autophagosomes (arrowheads). (**d**) Silver staining of A(α), B(β) and γ chains of human purified plasminogen-depleted > 99% clottable fibrinogen (left), and α, β and cross-linked γ chains of fibrin polymers (right) after separation on 4-12% reducing SDS-PAGE. Fibrin polymers were prepared as described in Methods. A(α) and B(β) chain of fibrinogen show somewhat higher mobility than α and β chains of fibrin because they contain fibrinopeptide that is cleaved by thrombin during preparation of fibrin. Fibrin does not have free γ chain as expected, but shows instead cross-linked γ chains. Representative of 5 independent replicates. (**e**) Transmission electron microscopy images of fibrin fibrils. Representative of 3 independent replicates. (**f**) Representative images of 3 independent replicates of MBP- and fibrin-double positive OLs. Orthogonal views show internalization of fibrin 6 h after treatment (0.1 mg/mL). Bar = 10 μm. (**g**) Western blots of autophagy markers LC3-I, LC3-II, and p62 in primary mouse OLs cell lysates after treatment with fibrin (0.1 mg/mL) or vehicle for 12 h with or without autophagy inhibitor MHY 1485 (2 μM). Western blots are representative of 3 independent experiments. (**h**) Quantification of live cells with live/dead assay 24 h after vehicle or fibrin (0.01-0.1 mg/mL) treatment of mature OLs. OLs were additionally treated with autophagy inhibitors MHY 1485 (2 μM) and inhibitor VII (100 μM). Hirudin (4 U/mL) was added to all cultures except for the grey filled circles which are vehicle-controls. Mean ± s.e.m.; n=5 independent experiments (each 3 coverslips per condition). (**i**) Representative confocal images of mouse pericyte cultures after treatment of live cells with CytoID autophagy kit (green, middle) followed by immunostaining for platelet-derived growth factor receptor β (PDGFRβ), a pericyte marker (red, left), and active form of caspase 3 (cyan, right) at 6, 12 and 24 h after treatment with vehicle, fibrinogen (1.5 mg/mL) or fibrin (0.1 mg/mL) with and without MHY 1485 (2 μM). Arrows point to formation of autophagosomes (bar = 10 μm). (**j, k**) Quantification of CytoID+ autophagic cells (**j**) and active Caspase 3+ cells (**k**) in mouse pericyte cultures 6, 12 and 24 h after fibrinogen (1.5 mg/mL) or fibrin (0.1 mg/mL) treatment with and without MHY 1485. Mean ± s.e.m.; n=5 independent experiments (each 3 coverslips per condition). (**l**) Quantification of live cells with live/dead assay 24 h after vehicle, fibrinogen (1.5 mg/mL) or fibrin (0.1 mg/mL) treatment of mouse pericytes. Pericytes were additionally treated with autophagy inhibitors MHY 1485 (2 μM) and inhibitor VII (100 μM). Hirudin (4 U/mL) was added to all cultures except for the grey filled circles which are vehicle-controls. Mean ± s.e.m.; n=5 independent experiments (each 3 coverslips per condition). In panels b, h, j, k, and l one-way ANOVA and Bonferroni's post hoc tests were used; ns=non-significant ($p>0.05$).

Supp. Figure 14

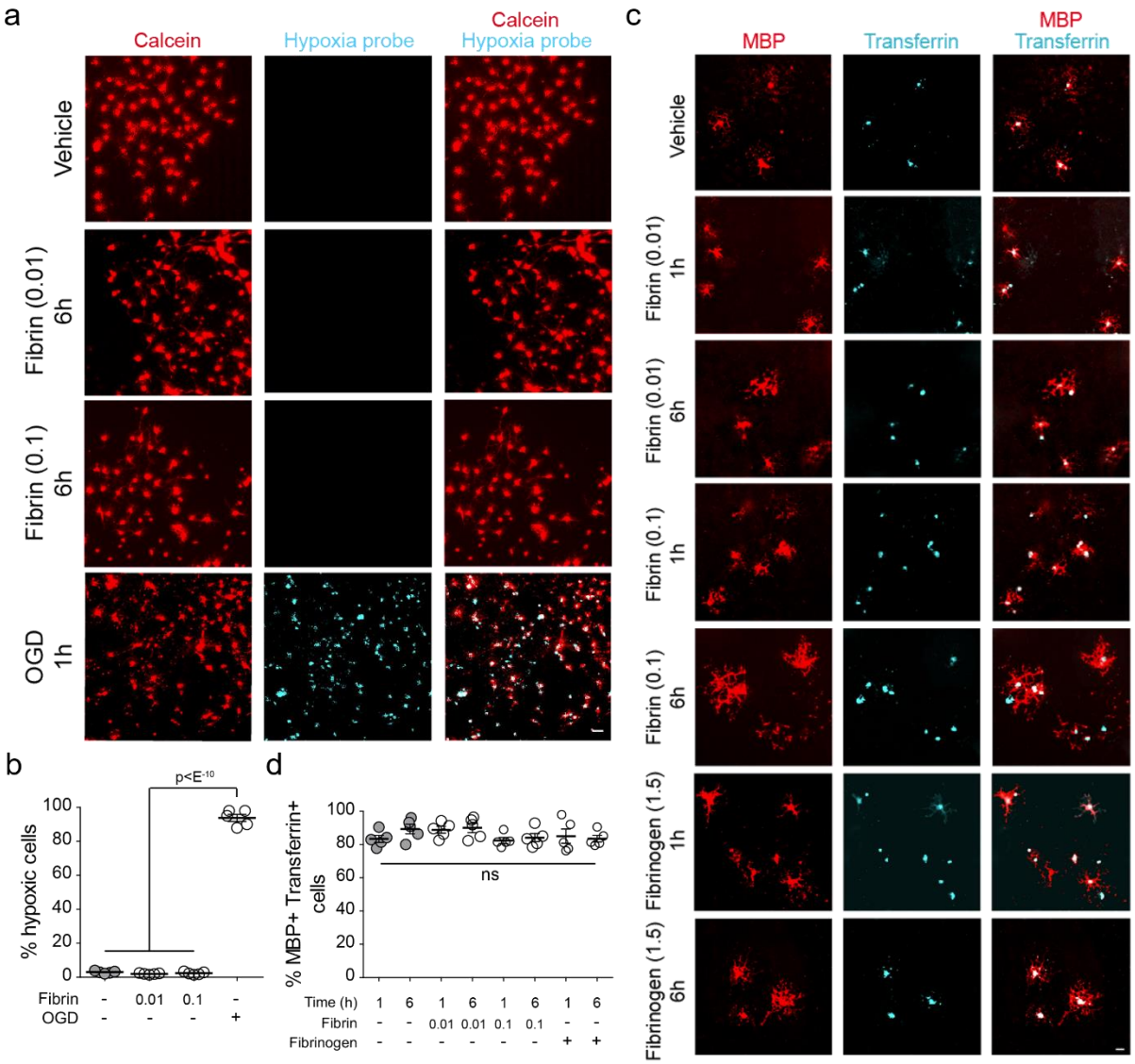

Supplementary Figure S14. Oxygen availability and transferrin uptake from the culture medium by mature oligodendrocytes after fibrin and/or fibrinogen treatment. (**a, b**) Representative confocal images (**a**) and quantification (**b**) of mature oligodendrocyte live cells labeled with calcein (red) that tested positive for hypoxia by Image-iT Hypoxia Reagent probe (5 µM, cyan) 1 h after oxygen-glucose deprivation (OGD, positive control) compared to no hypoxic cells after treatment with fibrin (0.01 and 0.1 mg/mL) or vehicle for 6 h (bar = 20 µm). Mean ± s.e.m.. (**c, d**) Representative confocal images (**c**) and quantification (**d**) of Alexa 594-conjugated transferrin (25 µg/mL; cyan) cellular uptake by MPB+ oligodendrocytes (red, left) 1 and 6 h after addition of fibrin polymers (0.01 and 0.1 mg/mL) or fibrinogen (1.5 mg/mL). Alexa 594-transferrin was added to cell cultures 20 min before indicated time points (bar = 10 µm). Mean ± s.e.m.. In b and d, n=5 independent experiments (each 3 coverslips per condition); one-way ANOVA and Bonferroni's post hoc tests were used; ns=non-significant (p>0.05).

Supp. Figure 15

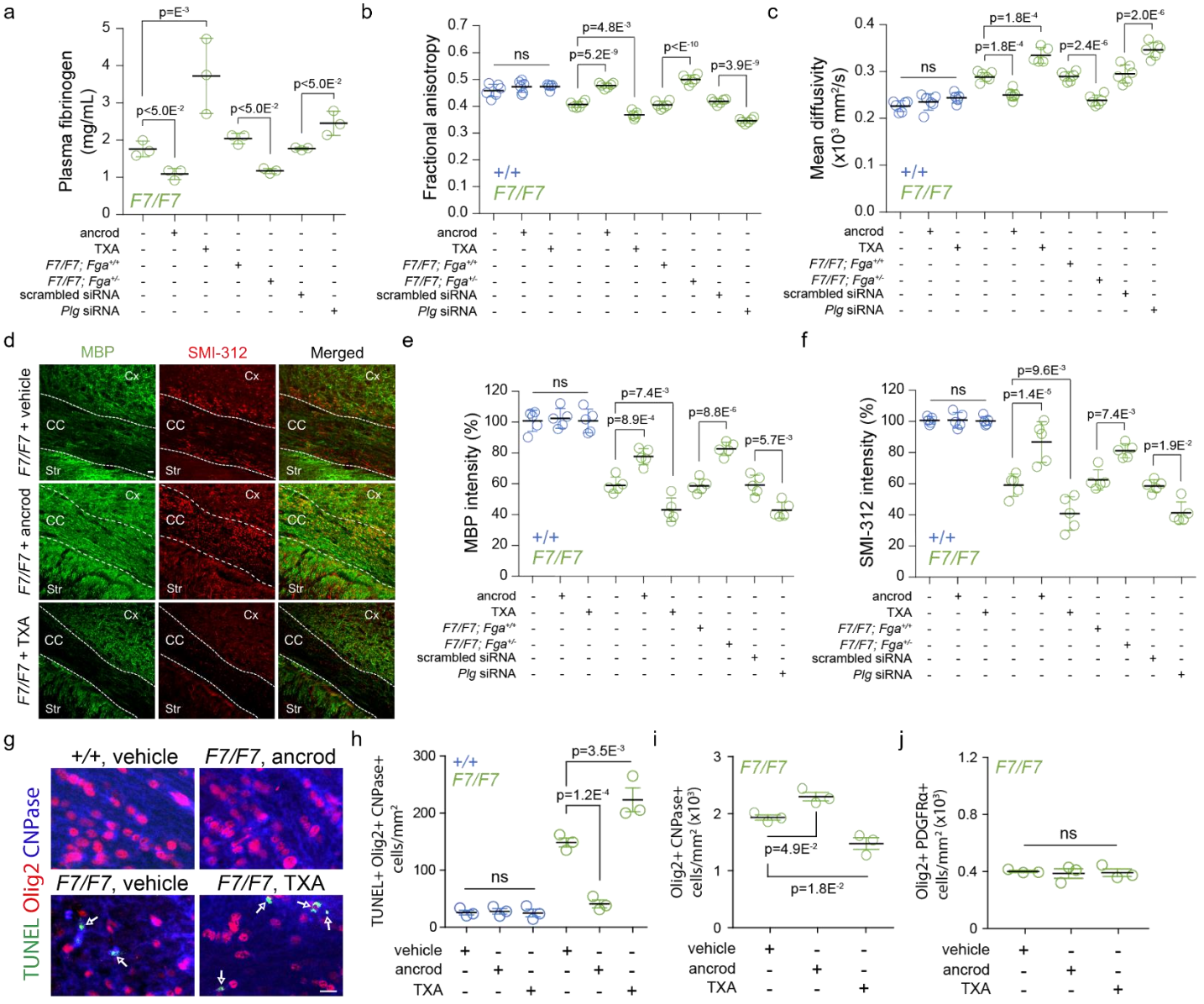

Supplementary Figure S15. White matter vascular damage and structural changes in pericyte-deficient mice after pharmacological or genetic manipulation of fibrinogen systemic levels. (**a**) Plasma fibrinogen levels in 12-week old *F7/F7* (green) mice treated with vehicle, ancrod or TXA, *F7/F7*; *Fib*$^{+/-}$ mice compared to *F7/F7*; *Fib*$^{+/+}$ littermate controls, and *F7/F7* mice treated with scrambled siRNA or *Plg* siRNA for 7 days. Mean ± s.e.m.; n=3 mice per group. (**b, c**) Fractional anisotropy (**b**) and mean diffusivity (**c**) in the CC of 12-week old *F7/F7* mice (green) and littermate controls (+/+, blue) mice. Values were generated from diffusion tensor imaging MRI scans. Mean ± s.e.m.; n=6 vehicle-treated +/+ and *F7/F7* mice; n=6 ancrod-treated +/+ and *F7/F7* mice; n=5 TXA-treated +/+ and *F7/F7* mice; n=6 *F7/F7; Fib*$^{+/+}$, *F7/F7; Fib*$^{+/-}$, *F7/F7* + scrambled siRNA, and *F7/F7* + *Plg* siRNA. (**d**) MBP (green) and SMI-312 (red) staining in the corpus callosum (CC) of vehicle- (*upper panels*), ancrod-treated (middle panels), and TXA-treated (*lower panels*) 12-week old *F7/F7* mice (bar = 20 µm). Cx, cortex; Str, striatum. (**e, f**) Quantification of MBP (**e**) and SMI-312 (**f**) immunoreactivity in the CC of 12-week old *F7/F7* (green) and littermate control (+/+, blue) mice. Mean ± s.e.m.; n=5 untreated +/+ and *F7/F7* mice; n=5 ancrod-treated +/+ and *F7/F7* mice; n=5 TXA-treated +/+ and *F7/F7* mice; n=5 *F7/F7; Fib*$^{+/+}$, *F7/F7; Fib*$^{+/-}$, *F7/F7* + scrambled siRNA, and *F7/F7* + *Plg* siRNA. (**g**) TUNEL-, Olig2- and CNPase-triple-positive oligodendrocytes in the CC of 12-week old +/+ and *F7/F7* mice treated with vehicle, ancrod or TXA (bar = 20 µm). (**h**) Quantification of TUNEL-, Olig2- and CNPase-triple-positive oligodendrocytes in the CC of 12-week old +/+ and *F7/F7* mice treated with vehicle, ancrod or TXA. Mean ± s.e.m.; n=3 mice per group. (**i, j**) Quantification of Olig2- and CNPase-double positive mature oligodendrocytes (**i**) and Olig2- and PDGFRα-double-positive oligodendrocyte

precursor cells (**j**) in the CC of 12-week old *F7/F7* mice treated with vehicle, ancrod or TXA. Mean ± s.e.m.; n=3 mice per group. In panels a, b, c, e, f, h, i, and j, data were compared by one-way ANOVA and Bonferroni's post hoc; ns=non-significant ($p>0.05$).

Supp. Figure 16

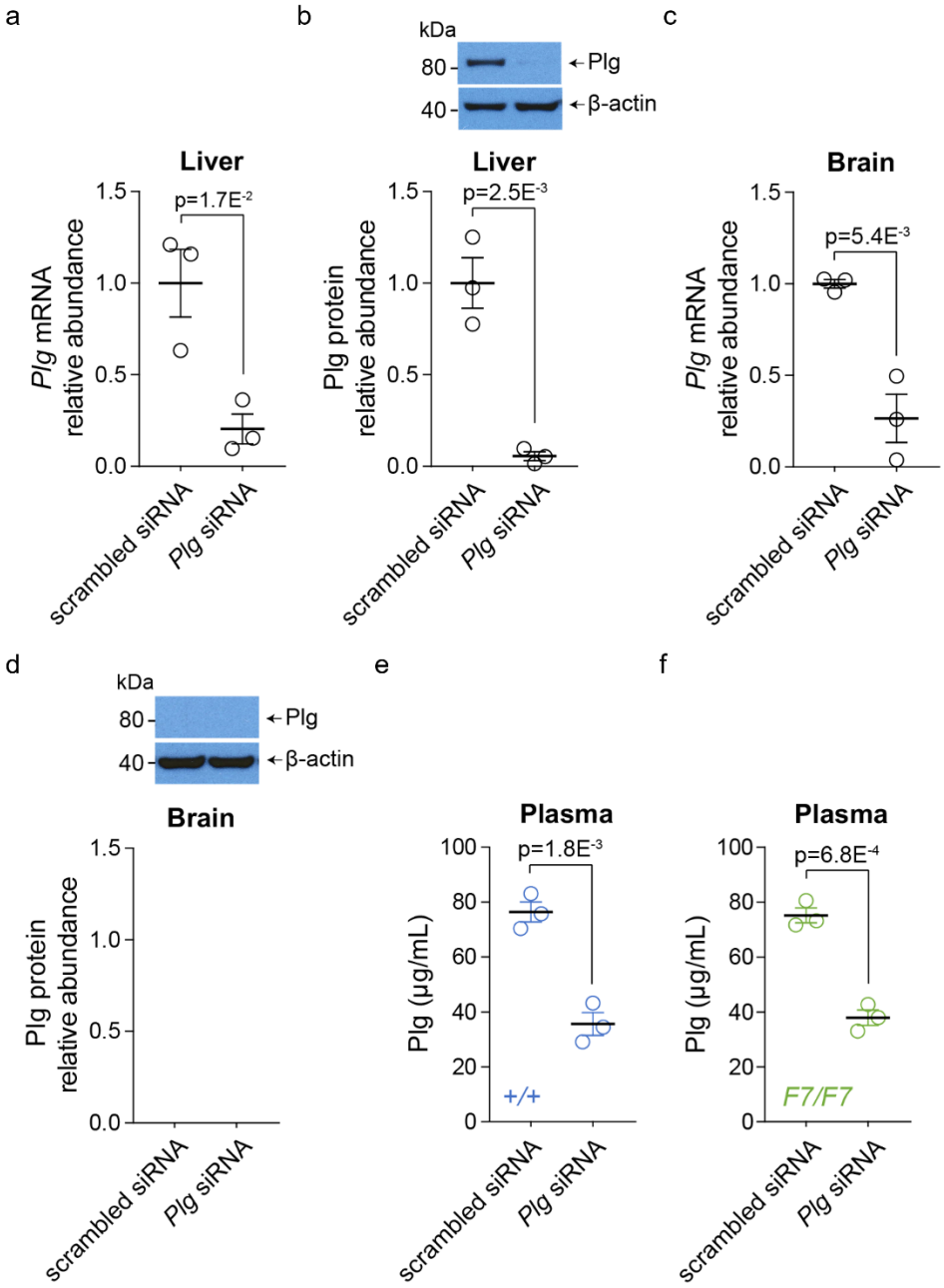

Supplementary Figure S16. Knockdown of plasminogen (Plg) in liver and brain after systemic and intracerebroventricular administration of *Plg*-specific siRNA compared to scrambled siRNA in 16-week old +/+ and *F7/F7* mice. (**a-d**) qRT-PCR analyses of *Plg* transcripts (**a**) and Plg protein (**b**) in the liver and brain (**c, d**) 2 days after administration of *Plg* siRNA compared to scrambled siRNA. (**e**) Plasma Plg levels 7 days after administration of *Plg* siRNA compared to scrambled siRNA in 16-week old +/+ mice. (**f**) Plasma Plg levels 7 days after administration of *Plg* siRNA or scrambled siRNA in 16-week old *F7/F7* mice.In all panels, mean ± s.e.m.; n=3 mice per group; for all panels, unpaired two-tailed Student's *t*-test was used for statistical comparisons.

Supp. Figure 17

Figure 4l

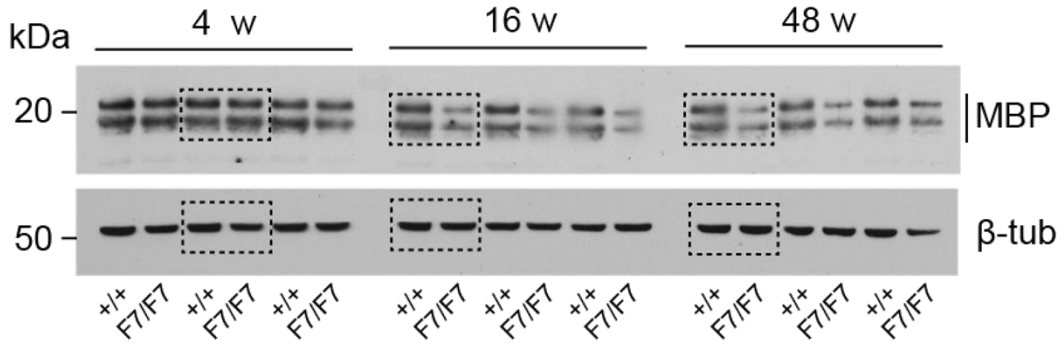

Figure 5n

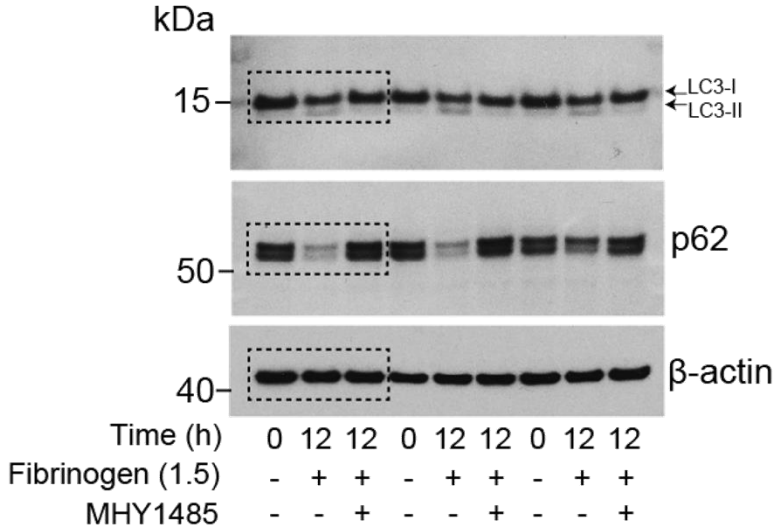

Supplementary Figure S17. Full scans of western blots. Full scans of western blots for MBP shown in Figure 4 panel l (*top*) and LC3-I, LC3-II, and p62 shown in Figure 5 panel n (*bottom*).

Supp. Figure 18

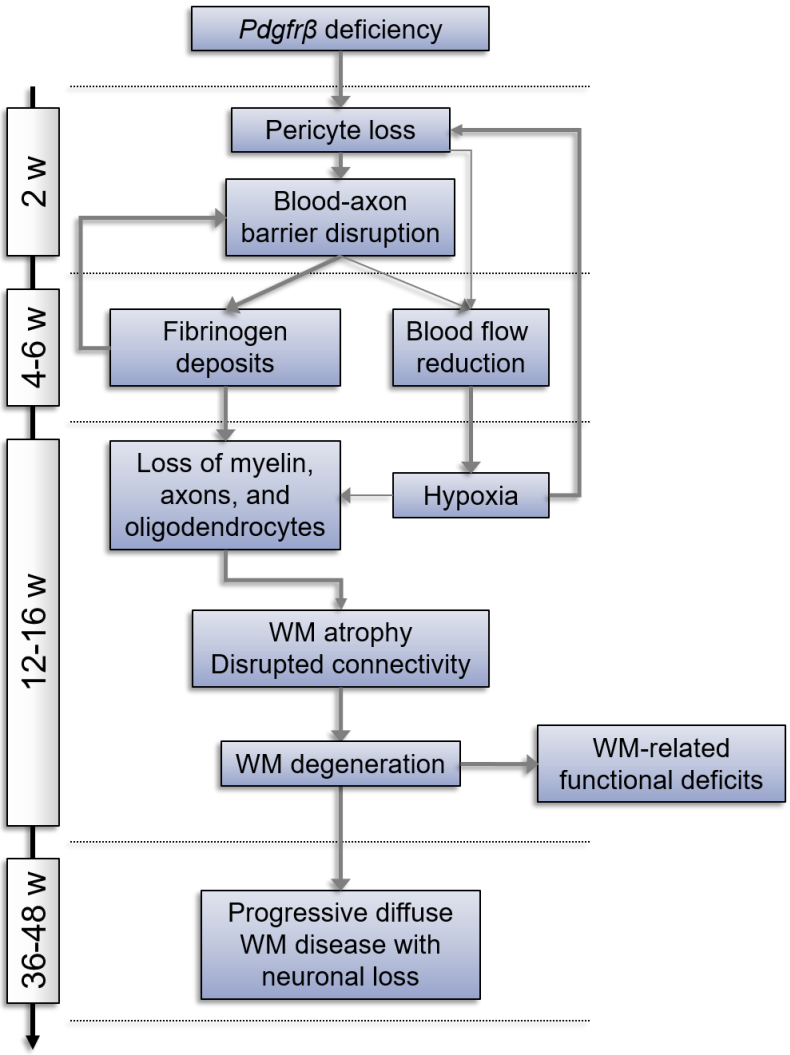

Supplementary Figure S18. A pathogenic cascade in pericyte-deficient *F7/F7* mice leading to white matter degeneration. Early pericyte loss induced by platelet-derived growth factor receptor β (PDGFRβ) deficiency leads to early disruption of white matter (WM) microcirculation and breakdown of blood-axon barrier integrity at 2 weeks of age causing WM accumulation of blood-derived toxic fibrin(ogen) deposits and blood flow reductions between 4 and 6 weeks of age. At that time, the WM structure and function appear normal as assessed by MRI volumetric and connectivity analyses, viral tract-tracing connectomic analysis, tissue immunocytochemistry and ultrastructural electron microscopy analysis, and behavior testing. Progressive vascular phenotype and the developing WM fibrin(ogen) deposits and hypoxia lead between 12 and 16 weeks of age to WM structural and functional degenerative changes with loss of myelin, axons and oligodendrocytes resulting in WM atrophy, loss of connectivity and WM-related functional deficits. At that time, no changes in grey matter (GM) volume and/or neuronal loss were observed on MRI, histological and/or functional analysis, respectively. However, the advancing small vessel disease and WM degeneration lead between 36 and 48 weeks of age to progressive diffuse WM disease with a substantial loss of WM volume associated with GM atrophy, neuronal loss and the corresponding behavioral deficits.

Supp. Figure 19

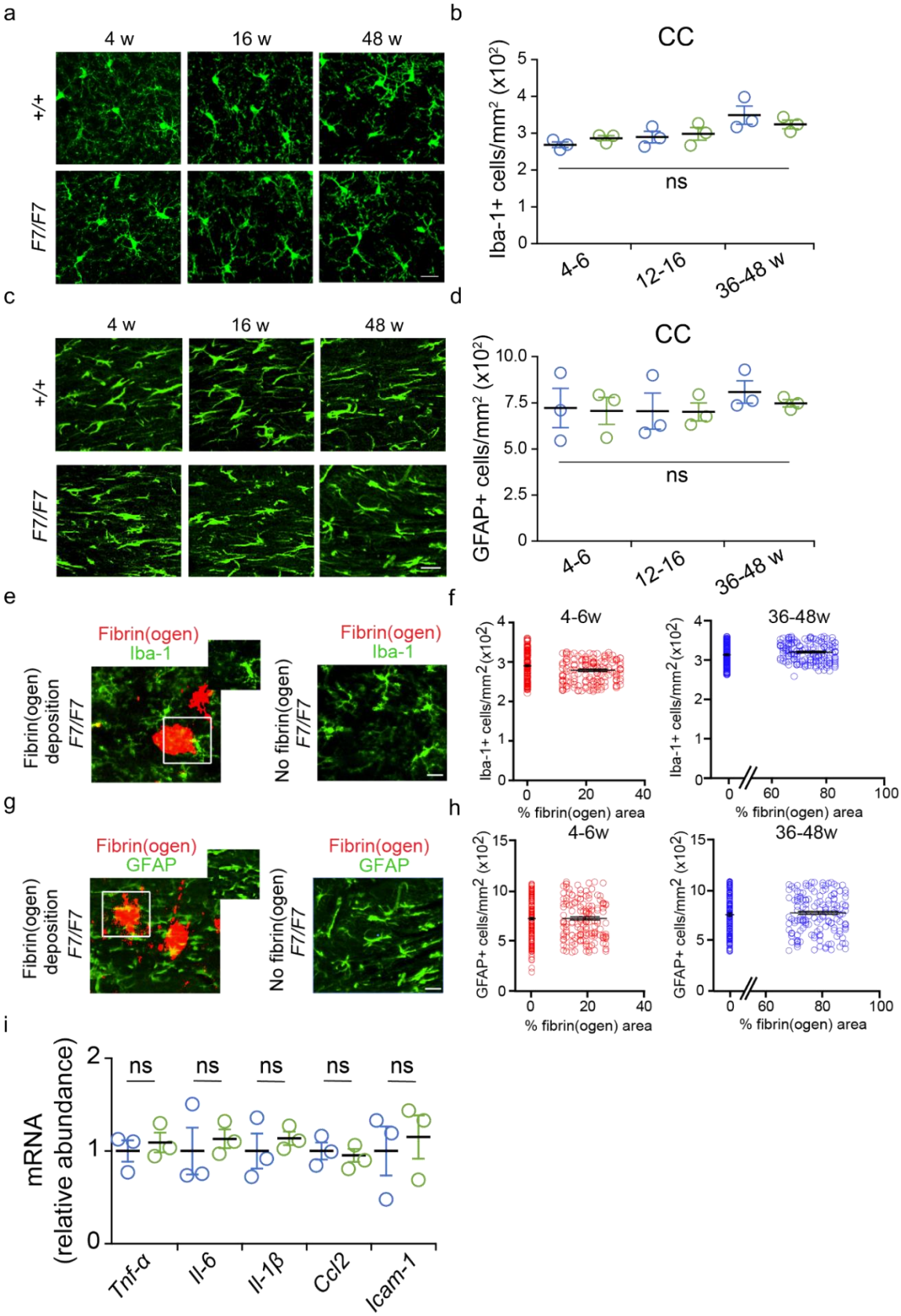

Supplementary Figure S19. Lack of neuroinflammatory response in the white matter during early stages of white matter disease in pericyte-deficient mice. (**a**) Confocal images of Iba-1-positive microglia in the corpus callosum (CC) of 4-, 16-, and 48-week old *F7/F7* and littermate control +/+ mice (bar = 20 µm). (**b**) Quantification of Iba-1-positive cells in the CC of 4-6-, 12-16-, and 36-48-week old *F7/F7* (green) and +/+ (blue)

mice. Mean ± s.e.m.; n=3 mice per group. (**c**) Confocal images of GFAP-positive astrocytic cells in the CC of 4-, 16-, and 48-week old *F7/F7* (green) and littermate control +/+ (blue) mice (bar = 20 μm). (**d**) Quantification of GFAP-positive astrocytic cells in the CC of 4-6-, 12-16-, and 36-48-week old F7/F7 and +/+ control mice. Mean ± s.e.m.; n=3 mice per group. (**e**) Confocal images of Iba-1-positive microglia in the CC of 48-week old *F7/F7* mouse in areas with fibrin(ogen) deposition (red, left) and without fibrinogen (right). Inset, Iba-1-positive microglia staining in an area with fibrin(ogen) deposition after removing the red channel (bar = 20 μm). (**f**) Quantification of Iba-1-positive cells in the CC of 4-6-week old (red) and 36-48-week old (blue) *F7/F7* mice in areas with and without fibrinogen deposition. In each mouse, 50 randomly selected 50 x 50 μm-sized boxes in areas with and without fibrin(ogen) deposition derived from 6 adjacent tissue sections 100 μm apart was taken for analysis. Mean ± s.e.m.; n=150 individual points per group in areas with and without fibrin(ogen) deposition from 3 mice per group. (**g**) Confocal images of GFAP-positive astrocytes in the CC of 48-week old *F7/F7* mouse in areas with fibrin(ogen) deposition (red, left) and without fibrinogen (right). Inset, GFAP-positive astrocyte staining in an area with fibrin(ogen) deposition after removing the red channel (bar = 20 μm). (**h**) Quantification of GFAP-positive astrocytes in the CC of 4-6-week old (red) and 36-48-week old (blue) *F7/F7* mice in areas with and without fibrinogen deposition. In each mouse, 50 randomly selected 50 x 50 μm-sized boxes in areas with and without fibrin(ogen) deposition derived from 6 adjacent tissue sections 100 μm apart was taken for analysis. Mean ± s.e.m.; n=150 individual points per group in areas with and without fibrin(ogen) deposition from 3 mice per group. (**i**) Messenger ribonucleic acid (mRNA) levels of tumor necrosis factor alpha (*Tnf-α*), interleukin 6 (*Il-6*), interleukin 1 beta (*Il-1β*), chemokine C-C motif ligand 2 (*Ccl2*), and intercellular adhesion molecule 1 (*Icam-1*) in the white matter homogenates of 12-16-week old *F7/F7* compared to littermate control +/+ mice. Mean ± s.e.m.; n=3 mice per group. In panels b and d, one-way ANOVA and Bonferroni's post hoc tests were used. In panels f, h, and i, unpaired two-tailed Student's *t*-test was used; ns=non-significant ($p>0.05$).